
Article:
Nikkhou, M, Gleeson, HF orcid.org/0000-0002-7494-2100 and Muševič, I (2018) Creation and topological charge switching of defect loops on a long fibre in the nematic liquid crystal. Liquid Crystals, 45 (13-15). pp. 2294-2305. ISSN 0267-8292

https://doi.org/10.1080/02678292.2018.1500653

INVITED ARTICLE

Creation and topological charge switching of defect loops on a long fibre in the nematic liquid crystal

M. Nikkhou[a], H. F. Gleeson[a] and I. Muševič[b,c]

[a]School of Physics and Astronomy, University of Leeds, LS2 9JT Leeds, UK; [b]J. Stefan Institute, Jamova 39, SI-1000 Ljubljana, Slovenia; [c] Faculty of Mathematics and Physics, University of Ljubljana, Jadranska 19, SI-1000 Ljubljana, Slovenia

ARTICLE HISTORY
Compiled August 8, 2018

ABSTRACT
We demonstrate new type of topological defects on a homeotropic fibre aligned perpendicular to the nematic director in a planar nematic cell. Contrary to expectations we can create defect loops which are encircling the fibre along its short axis and are strongly tilted with respect to the fibre. Such loops are always accompanied by two topological solitons, which emanate from the loop and propagate to the left and right hand side of the fibre. Unlike previously reported closed loops of either positive and negative charge, encircling the fibre parallel to the nematic director, these loops can carry either positive or negative charge, or can be charge neutral and very stable. We show how to switch the charge of individual loops from positive to neutral and negative charge by adding unit monopoles of appropriate topological charge. We demonstrate new type of interaction of dipolar colloids with these new topological entities on a fibre.

KEYWORDS
Microconfined liquid crystals; topological defect; homeotropic fibre; colloidal interaction; entanglement; anchoring; liquid-solid interfaces

Dataset: https://doi.org/10.5518/401

1. Introduction

The creation and manipulation of topological defects has attracted widespread attention as they have been shown to play an important role in physical and biological systems [1–3]. These excitations arise spontaneously during the symmetry-breaking phase transitions and appear through the Kibble-Zurek mechanism of defect production [4,5] in soft ferromagnetism [6–8], super-fluidity [9,10], super-conductivity [11], liquid crystals [12,13] and the Universe [4,5].

In nematic liquid crystals (NLCs) topological defects appear in a form of closed loops and points and are characterized by their winding and topological charge [14–18]. The molecular orientation is not well defined at the core of a defect, which is a nanometer-size region of decreased orientational order. This singular core is surrounded by a strongly distorted nematic director field which is of a typical dimension

CONTACT M. Nikkhou. Email: m.nikkhou@leeds.ac.uk

of several micrometers due to the softness of the liquid crystal. Because liquid crystals are optically birefringent, the strongly orientationally distorted region around the topological defect is optically very inhomogeneous, which makes them optically easily visible under an optical microscope [19]. Defects in nematic liquid crystals are quite large and soft, they are easily created and manipulated by external stimuli, such as the strong laser light of the laser tweezers.

There are two most common kinds of point defects in the nematic liquid crystal: the radial hedgehog which by convention carries a positive unit topological charge $q = +1$, and the hyperbolic hedgehog carries a negative unit charge $q = -1$ [14–17]. The attribution of a sign to a particular unit charge hedgehogs is quite consistent in most experimental realizations, such as 2D spherical colloids, but faces ambiguities [13] in some topologically more complex cases. One example is a toroidal handlebody with perpendicular surface anchoring, where two hedgehogs of the same hyperbolic structure have to be assigned two different signs of their unit charge [20]. These cases have to be treated with care when assigning the vector direction to the director field, which does not influence the overall conservation of the topological charge. The hedgehogs of higher unit charges have recently been observed in chiral nematic droplets by fluorescent imaging [21,22]. The hedgehogs are actually quite rare in bulk nematic liquid crystals, they appear more often in chiral nematic droplets, capillaries and thin layers of the nematic liquid crystal. They are particularly abundant in nematic colloids, where they are topologically protected by the law of conservation of topological charge and are associated with each colloidal inclusion. When foreign particles are introduced into the nematic liquid crystal, defects are spontaneously created at each particle to compensate for the molecular alignment along the closed surface of the inclusion [16]. The nature of particle-induced defects depends on the particle topology [20,23–27], the type of surface anchoring and confinement [28–33] and they can be transformed one into another [31,34]. Topological defects and the resultant particle-induced deformations in the nematic director give rise to strong forces between colloidal particles, and with curved director fields [35], and these forces are of elastic origin. These interactions are long range, anisotropic, and lead to various types of structures such as linear [36–39] and kinked [34] chains of colloidal particles, two-, and three-dimensional colloidal crystals [33,34,39–43].

Rods, cylinders and fibers are of the same form as the spheres from the standpoint of topology and they both have the genus g=0 [20]. The topology of the particle is determined to the largest extent by the genus of the particle, which counts the number of "holes" through the particle, or the number of "handles" attached to the particle. Colloidal particles with genus zero, say, spheres and cylinders with normal surface anchoring inserted into a homogeneous bulk nematic liquid crystal (NLC), will give rise to a single hyperbolic hedgehog point defect or a single disclination ring, carrying the topological charge of $q = -1$. The topological charge of the accompanying defect will compensate the topological charge of the surface of the inclusion so the overall charge remains zero at all times.

The conservation of the total topological charge does not constrain the number of defects, which are actually created on an object in the NLC. Namely, additional pairs of defects can always be created as long as their total topological charge is kept to zero. This was first demonstrated in a series of experiments with long fibers inserted in the NLC [26,44–46]. Using the laser tweezers one is able to create pairs of oppositely charged topological defects, cut them into smaller entities, merge them into larger entities etc... Long fibre included in nematic nematic liquid crystals has emerged as a perfect setting to prove and observe the basic laws of topology in two dimensions.

A topological soliton in the nematic liquid crystal is a smooth but a topologically nontrivial spatially localized structure embedded into a uniform nematic background. Some of the earliest observations of topological solitons in liquid crystals were strings of uniform width, connected to boojums at their ends [47–49]. The string-like soliton generates a constant string-like force of attraction between the two boojums at each end of the string and consequently constant velocity of the defects during their attraction. Previous studies on the topological solitons were focused on the creation and the stability of nonsingular solitonic structures and the resultant deformation in the director field. In different experiments the stability of the soliton obtained by electric field [50], colloidal particles [44], film thickness gradient and the surface anchoring was studied [51,52]. We have recently reported on the creation of a linear topological soliton on a long, micrometer-diameter glass fibre in a NLC film in which the fibre was set perpendicular to the bulk orientation of the NLC [45]. The focus of that study was the creation of hedgehogs of opposite topological charge on the fibre and their annihilation dynamics, which demonstrated a Coulomb-like elastic attraction between the hedgehogs at short separation.

In this work, we demonstrate the interaction between a defect loop encircling the fibre's short axis with point monopoles, created by the light of the laser tweezers on solitonic structures in the vicinity of the fibre. The loop is either charge-neutral or has topological charge of +1 or -1. Two solitons, one on the bottom and the other on the top of the fibre, can meet each other at this topological loop. We show how the monopoles on both solitons are attracted to the oppositely signed end of the loop, changing the loop sign from negative to neutral and neutral to positive, and vice versa. This provides novel method of controlling the sign of the loop by light of the tweezers. We also study assemblies of microspheres with the fibre by entangled defects. By switching the sign of the loop, the colloidal entanglement changes and therefore the assembled structures can be manipulated. This opens new avenues in the design of tunable colloidal superstructures, and may thus serve as controllable photonic materials.

2. Materials and experimental techniques

Glass micro-fibres of diameter 8-12 μm were used in the experiments. These fibres are made by heating a 125 μm optical glass fibres with oxygen-hydrogen torch and mechanical stretching to obtain a desired fibre diameter. To achieve very strong homeotropic anchoring of NLC on the surface of fibres, clean fibres were immersed in 2 vol% solution of octadecyldimethyl (3-trimethoxysilylpropyl) ammonium chloride (DMOAP silane, ABCR GmbH) in water for 5 min and then rinsed with deionized water for few minutes to remove the excess of silane. The fibres were blown with dry Nitrogen (N_2) and then were left in an oven at 120°C for 30 min. The fibre from the tapered end was introduced into a cell of thickness 15-20 μm and was cut to a length of 300-600 μm. The cells were made of two glass plates covered with an optically transparent indium tin oxide (ITO) layer, with the inner surfaces modified to ensure either good planar or homeotropic alignment. To achieve planar alignment, the glass plates were covered by a thin layer of polyimide (PI 5291, Brewer Science). The plates were antiparallel rubbed using a rubbing machine to ensure excellent planar alignment of the LC molecules. In order to get homeotropic alignment, the glass plates were silanized in a similar way to that described for the fibres. The ITO coating on the inner side of the substrate provides very good control of the local heating of the LC by absorption of

the laser-tweezers light. The gap between the glass plates was maintained with mylar spacers and the cell glued with two component epoxy glue (UHU, GmbH or Torr Seal, Varian). The cell thickness was measured by a standard interference technique, using spectrophotometer (USB2000, Ocean Optics). On filling the cell with the 4-pentyl-4-cyanobiphenyl (5CB, Merck) NLC, the fibre moves inside the cell through capillary force from the LC flow. In the experiments with the planar cell, the long axes of the fibres were oriented perpendicular to the rubbing direction using laser tweezers. In the case of the homeotropic cell, the long axes of the fibres were always perpendicular to the bulk orientation of the NLC, therefore the orientation of the fibres was not important. In some of the experiments, silica microspheres with 10 μm diameter (Duke Scientific), also with homeotropic surface anchoring, were immersed into the same cell. A laser tweezers setup with an infrared fibre laser operating at 1064 nm built around an inverted microscope (Nikon Eclipse, TE2000-U), was used as a light source. The trap manipulation was controlled with a pair of acousto-optic deflectors driven by computerized system (Aresis, Tweez 70). The images were recorded using a Pixelink PLA 741 camera.

3. Topological soliton

Here we describe the creation and stabilization of an escaped topological soliton in the NLC by colloidal particles. The fibre with the homeotropic surface anchoring of NLC is inserted into the planar cell, and is set perpendicular to the rubbing direction. In the experiments with homeotropic cells the fiber was inserted into the cell without any particular in-plane orientation, because the orientation does not matter in this geometry. Left and right panels in Fig. 1 (a) show the orientation of the fibre and of the nematic liquid crystal director in a planar and a homeotropic cell, respectively. The cell is in the x-y plane, whereas the z-axis is pointing perpendicular to the nematic liquid crystal layer.

In the first experiment, the fibre is set perpendicular to the rubbing direction in a planar nematic cell with a cell gap of 20 μm. A gigantic -1/2 Saturn ring is stretched all along the length of the fibre, which is clearly observed under an optical microscope, as shown in the first panel of Fig. 1 (b). We have recently shown how this gigantic Saturn ring can be cut and reshaped using the localized and very strong beam of the laser tweezers [26]. Fig. 1 (b) briefly illustrates the procedure of cutting the Saturn ring into two separate parts. When the laser beam is focused on the NLC of one side of the fibre, an island of molten (isotropic) NLC is created as shown in the second panel of Fig.1 (b). We can grab the ring by the isotropic island and pull it down. After switching off the light, a dense tangle of topological defects appears, similar to the Kibble-Zurek mechanism of defect creation [5,53,54]. In less than a second, this tangle annihilates and leaves behind two loops with opposite winding numbers, which are connected to one another through a narrow region of an escaped disclination called the "topological soliton". Since the topological charge of gigantic Saturn ring is by convention assigned a -1 unit charge, one of the loops created after the cut has a charge of -1 and the other must be charge neutral to preserve the conservation of the total topological charge of the system.

In Fig. 1 (c) the loop on the left side is charge neutral, whereas the loop on the right side is of negative charge. The winding number of the charge-neutral loop on the left of Fig. 1 (c) is +1/2, whereas the winding number of the right loop is -1/2. The two ends of the loops are connected with an escaped topological soliton, which

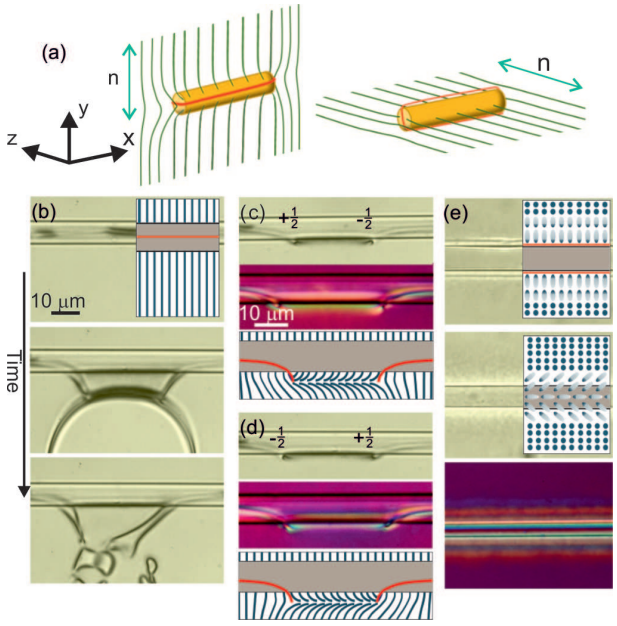

Figure 1. (a) Schematic drawing of the fibre perpendicular to the rubbing direction in a planar cell (right panel), and the fibre in a homeotropic cell (left panel). The x axis is along the long axis of the fibre, the y axis coincides with the liquid crystal director and the z axis shows the viewing direction, i.e. perpendicular to the measuring cell. (b) The fibre is set perpendicular to the rubbing direction in the nematic planar cell, and a gigantic Saturn ring is created encircling the fiber along the long axis. The ring is cut into two separated rings by the focused beam of laser light. (c) and (d) The loops obtained after cutting the Saturn ring are separated by a smooth region with splay-bend deformation known as a "topological soliton". The second panels were taken under cross polarizer with a λ wave-plate, which is inserted at 45 degrees with respect to polarizer P and crossed analyzer A. The blue and yellow colors show the reversed director field in the vicinity of the fiber. The third panels show the schematic drawing of the director field within the soliton. (e) The fibre is inserted into the homeotropic nematic cell. The -1/2 Saturn ring is encircling the fibre in the plane of the paper (first panel) and appears as a thin thread. The inset shows schematic drawings of the orientation of nematic director. The second panel shows the escaped soliton above the surface of the fibre. The nematic director orientation is shown schematically (the inset of the second panel), and using the λ wave-plate (third panel).

is propagating the "topological flux" from one type of the monopole to another. The direction of propagation of the topological flux is reversed in Fig. 1 (d), where the local windings of the loop ends are reversed as well.

The reason for this particular occurrence of the two loops at both ends of the escaped solitonic structure is the tilt of the fibre from the exact perpendicular direction to the bulk orientation of the NLC. Because of this slight tilting, the elastic distortion of the soliton structure in between the loops becomes slightly asymmetric, depending on the direction of the escape. The loops after the cut are created in a way that seeks the minimum of the elastic energy and minimizes the energetically high-cost region. This will determine the winding and charge of the two loops on the righ and left-hand side of the soliton.

The configuration of the director field within the escaped soliton is shown in Figs. 1 (c) and (d) by using the λ wave-plate (the second panels) and illustrated by the schematic drawings (the third panels). The effect of this small offset of the orientation of the fibre with respect to far field director was also observed in our previous work on the annihilation dynamics of the monopoles on topological soliton [45].

Determination of the sign of the topological charge of the loops was described elsewhere [26,46]. Briefly, a small test particle such as micro-sphere, treated for perpen-

dicular surface anchoring, is released next to the loop. By convention, the sphere is assigned a +1 topological charge, whereas the accompanying hyperbolic hedgehog is assigned a -1 unit topological charge. It has been well demonstrated in previous experiments that the equally charged part of sphere and the loop repel each other and the oppositely charged parts attract. This helps us to unambiguously determine the charge and winding of the loop or even winding of local section of the loop.

The experiments were also performed for a fibre in a cell with homeotropic alignment of NLC as shown in Fig. 1 (e). In this case the loop(s) are positioned on top or below the fibre. By focusing the microscope on top of the fibre, one can easily observe the Saturn ring, which starts on the top of the fibre along its entire length and continues below the fibre connecting itself into a loop (Fig. 1 (e), first panel). The inset to the panel presents schematic drawings of the director. The Saturn ring can be cut into two loops as in the experiments in the planar cell. Fig. 1 (e), second panel, shows the soliton between the loops which is located in the front of the fibre. The local orientation of the molecules within the soliton can be determined using the λ wave-plate, as shown in lower panel of Fig. 1 (e).

4. Novel topological entities within the topological soliton

Fig. 2 (a) shows an experiment on a charge-neutral defect loop on a fibre oriented perpendicular to the far field nematic director in a planar cell. This charge neutral loop is created from the topological soliton, i.e. from the vacuum with no topological charges, and the procedure for creating a charge neutral loop out of a topological soliton is explained in detail elsewhere [26,46]. One should note that this loop is not encircling the fibre along its short axis, but starts and ends on the same side of the fibre. For this reason, this loop is quite unstable and can easily shrink to vacuum. In the next step, we cut this charge neutral loop by the laser tweezers and there are two possible outcomes, shown in Fig. 2 (a). Let us remember that the charge neutrality has to be preserved at all times, which means that the total topological charge of newly created topological objects has to be zero.

In the first case two tiny charge-neutral loops are created, which independently annihilate with time by shrinking to vacuum (Fig. 2 (a), bottom panel) and disappearing. In the second case a pair of -1 and +1 loops is created, which shrink into -1 and +1 monopoles (Fig. 2 (a), right panels). These two monopoles are quite stable if they are not allowed to move towards each other. However, if they are allowed to attract and move, they will annihilate into the vacuum, again preserving the total topological charge at all times.

In the second experiment shown in Fig. 2 (b) we create an isolated -1 topological loop on a fibre, as shown in the first panel of Fig. 2 (b). This loop was created by quenching the zero charge loop, as just described in Fig. 2 (a). The +1 loop is not shown on this image, but is present in the vicinity. By using the laser tweezers, the NLC in the vicinity of this -1 loop is locally heated into the isotropic phase. By carefully moving the optically-induced isotropic island towards the upper side of the fiber (see the second panel in Fig. 2 (b)), one can grab the loop and also move part of it to the other side of the fibre. At that position the tweezers is shut down, as shown in the third panel of Fig. 2 (b).

One can see from the fourth panel in Fig. 2 (b), that we have created two new loops. Unlike the original -1 loop shown in the first panel, these two new loops are encircling the fibre along its short axis. They are both strongly tilted towards each

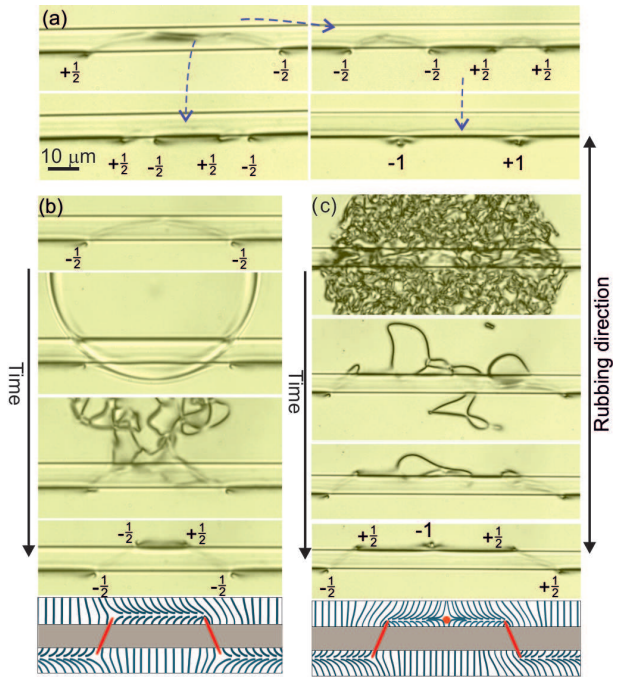

Figure 2. (a) The fibre is oriented perpendicular to the nematic director in a planar cell. A charge-neutral loop propagating along the fibre can be created out of the soliton. This charge neutral loop can be cut into two loops. These are either two charge-neutral loops, as shown in the bottom panel, or are two loops of opposite charge, which can spontaneously shrink to the point monopoles (the right panels). (b) Using optical tweezers the loop can be manipulated such that it is cut and split into two separate defect loops encircling the short axis of the fibre. Three solitons, two on the bottom and one on the top of the fibre can meet each other at topological loops. (c) By quenching the NLC around the soliton, a charge-neutral loop along fibre short axis, a -1 point defect and a +1 loop are created. The videos can be downloaded from dataset.

other, with the tilt angle close to 45°. This tilt can be understood by considering the director structure around the Saturn ring, which prefers to be oriented with its plane perpendicular to the far field director. In our case the far field director is perpendicular to the fibre, which forces the two loops to orient away from the director and stabilize at an angle of nearly 45°.

Because the total topological charge has to be preserved, these two loops must have total topological charge of -1. This is only possible if one of the loops has a -1 topological charge and the other loop must be of zero topological charge. The corresponding schematic structure of the director is shown in the fifth panel of Fig. 2 (b). It is clear that this cut locally changes the winding number of one of the loops from -1/2 to +1/2 and creates one stable charge-neutral loop. On the other hand it preserves the -1 loop and its winding characteristics. It is quite interesting to notice the power of the law of conservation of the overall topological charge, which forces the director structure of the nematic defect loops to comply to the law.

The sign switching of one of the winding of the loops encircling the fibre results in the formation of a new topological soliton, which now appears on the other side of the fiber, as shown in the fifth panel in Fig. 2 (b). One can see very clearly from this schematic panel, that we have alternation of the direction of escape of topological soliton, as we move along the fiber. The escaped soliton on the far left side changes the side of the fiber and at the same time it changes the direction of the escape, as we move towards the right and across the -1 loop. After traversing the zero charge loop the topological soliton flips back to the lower side of the fiber but preserves the direction of escape, because the local winding has changed.

Topological diversity of defects that could be created by laser quenching the liquid crystal around the fibre in planar cell is even richer, when we quench a topological soliton, i.e. "topological vacuum" with no defects. This is illustrated in the third experiment, shown in Fig. 2 (c). Before the quench, the topological soliton was on the lower side of the fibre in the first panel of Fig. 2 (c). Let us remind that this region of the topological soliton has zero topological charge, which has to be preserved regardless of the type and number of defects that we create out of that soliton. After the quench we see in the fourth panel of Fig. 2(c) two loops encircling the fibre, with a point monopole in the middle. The topological charge of this monopole was determined to be -1, which means that the topological charge of the two loops must add up to +1. This is only possible if one of the loops carries a +1 charge and the other loop is charge neutral. The schematic illustration of the corresponding director field is shown in the fifth panel of Fig. 2 (c).

These experiments clearly demonstrate how the position of the soliton can change in a fraction of a second and how topological entities such as charged or neutral loops and hedgehogs could be created by the quench. A simple fibre in the nematic liquid crystal therefore provides a fertile ground for creation and reconfiguration of topological defects. The process of creation and modification of defects in all cases follows the law of the conservation of total topological charge and winding in 2D.

We have also analyzed the creation of diclination loops and point monopoles within a topological soliton in a homeotropic cell (Fig. 3). Whereas in planar cell defects appear on the microscope image on each side of the fibre, they appear above and below the fibre in the homeotropic cell. The combined experiments in planar and homeotropic nematic cells therefore allow for more complete visualisation and analysis of defects because we are viewing them from two different angles in two different geometries.

Fig. 3 (a) shows a pair of -1 and +1 defect loops, which are obtained after the quenching the region of topological soliton in the homeotropic nematic with a fiber.

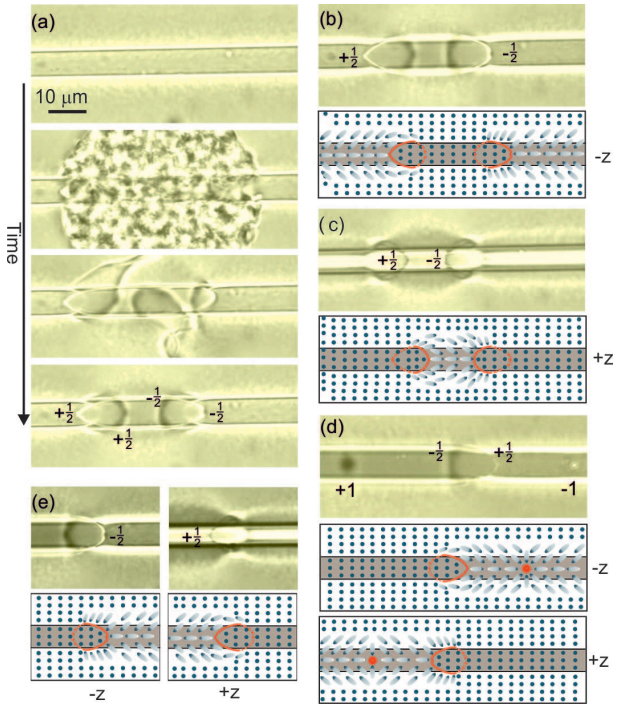

Figure 3. (a) Fibre in homeotropic cell of a NLC. A pair of +1 and -1 loops are created, encircling the fibre along its shorter axis. (b) and (c) show the defect loops in different focus. In the second panels the schematic drawing of the director field are shown. (d) A combination of point monopoles and charged-neutral loop can also be created on the soliton. Bottom panels show the schematic drawing in two different focuses(e) Non-polarized images (top panels) and the schematic drawing (bottom panels) of the charge-neutral loop are taken for different positions of the focus. The focuses on the front and the back sides of the fibre are shown by -z and +z axes, respectively.

They appear as closed loops of elliptic shape, which is due to their nearly 45° tilt, as we have seen in the other geometry, for example in Fig. 2 (b,c). The soliton was prepared as previously shown in Fig. 1 (e) by cutting the gigantic Saturn ring, which creates two separated loops with a topological soliton in between. Because the soliton is the region with zero topological charge, creation of two separate loops necessarily implies that their topological charges are opposite. In Fig. 3 (b) and (c) the objective is focused either in the front (b) or the behind (c) of the fibre, to clearly show the endings of the loops.

Similar to the fibre in a nematic planar cell, we demonstrate that various topological entities can be generated on that side of the fibre, where the soliton is present. The only rule to be obeyed is the conservation of the total topological charge. Fig. 3 (d) shows an example of a charge-neutral loop and two point monopoles created in another quench on the fibre. The loop switches the position of the soliton from one side to the other and a +1 point defect is created behind the fibre, while the -1 point defect is created in front of the fibre. The ends of the charge-neutral loop are shown in Fig. 3 (e) by focusing the objective on the front and back surfaces, respectively. The front and back sides of the fibre are opposite points on the z-axis, as illustrated in the left panel of Fig. 1 (a).

5. Switching the topological charge sign of disclination loop

Next step in the experiments is to investigate and demonstrate the switching of the sign of topological charge of disclination loop, which was created from the topological soliton on the fibre in the homeotropic cell. Two solitons, one placed behind and the other in front of the fibre, can meet each other at a topological loop encircling the fibre in a homeotropic cell as shown in Fig. 4 (a). This loop is charge-neutral, with -1/2 and +1/2 windings of the end sections of the loop behind and in front of the fibre, respectively.

We now analyze the interaction between this disclination loop and the additional point monopoles, which were created by the tweezers quenching in the vicinity. As opposite topological charges (windings) generally attract in 2D, the -1 point defect in the front of the fibre is attracted towards the positive end of the loop and when it interacts with the loop, it gets "absorbed" by the loop and correspondingly changes the winding number of that loop ending from +1/2 to the -1/2 (Fig. 4 (b)). This has an overall effect on the charge of the loop, which changes from neutral charge to -1 unit topological charge. On the other hand, the +1 point defect behind the fibre is also attracted to the opposite-signed end of the loop (-1/2 winding) and changes the winding number of the loop locally from -1/2 to +1/2, as shown in Fig. 4 (c). The total charge of that loop will change again from negative to neutral, because a unit positive charge was absorbed by the loop. The interaction between the point monopoles and the disclination loops therefore provides a versatile method of modifying the loop topological charge from negative to neutral and neutral to positive, and vice versa, in a fully controllable way.

6. Tuning colloidal dimers

We now focus our attention to the interaction of micro-spheres with loops and points, created by quenching the topological solitons. Microspheres with homeotropic surface

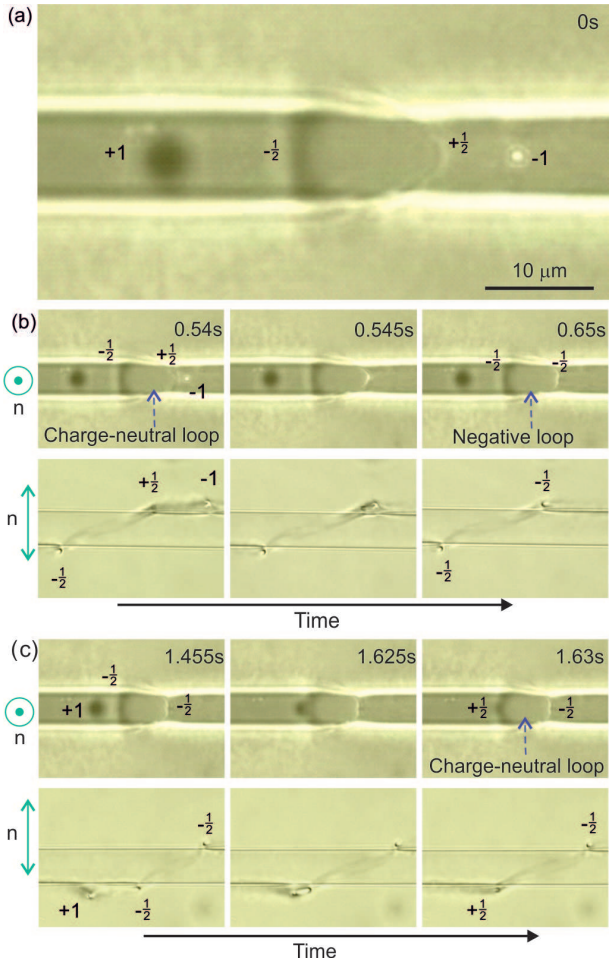

Figure 4. (a) A charge-neutral loop is encircling the fibre in the homeotropic cell, the -1/2 and +1/2 ends are on top and bottom of the fibre, respectively. The +1 and -1 point monopoles behind and in the front of the fibre, were also created from the topological soliton. (b) The -1 point defect (bright dot) is attracted to the end of the loop with a winding number of +1/2 and when being absorbed by the loop changes the overall charge of the loop from neutral to negative. Bottom panels show the same process in a planar cell. (c) The +1 point defect (dark dot) is attracted to the end of the loop with a winding number of -1/2. When absorbed by the loop it changes the charge of the loop from negative to neutral. Bottom panels show the same process in planar geometry.

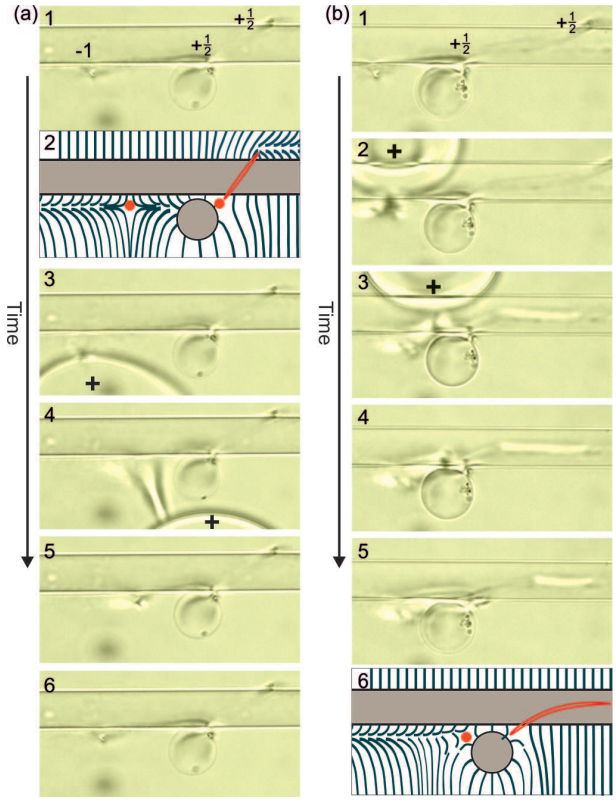

Figure 5. (a) The micro-sphere is spontaneously bound to the +1/2 end of the loop with its -1 hedgehog. An additional -1 point defect is created on the left-hand side of the microsphere, the schematic drawing of the director and defects is shown in the second panel. The -1 point defect is pushed along the fibre using the laser tweezers. The black crosses indicate the focus of the laser tweezers. When released, the -1 point defect is clearly repelled from the microsphere and the defect loop (fifth and sixth panels). The repulsive force due to the elastic deformation around the sphere is very strong and monopole can not approach the entangled defects. (b) We grab the -1 point defect with tweezers positioned on the other side of the fibre and push it towards the microsphere-loop joint. In this case the -1 monopole will interact with the -1 point defect of the microsphere and transform into a vortex-like binding, also known as "bubble gum" binding.

anchoring of NLC are well known to interact strongly with topological defects via dipolar or quadrupolar colloidal forces or via the colloidal entanglement [16]. These forces are of elastic origin and are also called structural forces. The entanglement of topological objects and defects is usually enforced by heating locally the NLC into the isotropic phase and then rapidly cooling it down, as described in our previous work [46]. Briefly, the nematic liquid crystal in the vicinity of the disclination loop around the fibre and the micro-sphere is locally heated using laser tweezers into the isotropic phase and then quenched back to the nematic phase by switching-off the laser. When passing through the isotropic-nematic phase transition, a dense tangle of defect loops is created that promptly annihilate, leaving behind different entangled defect structures. These entangled structures can be reconfigured and tuned by topological point defects as we shall demonstrate in Fig. 5 and Fig. 6.

The binding and entanglement of the topological point defect of a micro-sphere with the far segments of the loops, which have a local winding number +1/2, is shown in Fig. 5. We show in the first panel of Fig. 5 (a) that the far segment of the loop with local winding number of the +1/2 is attracted to the -1 hyperbolic hedgehog of the micro-sphere. The micro-sphere and the fibre are bound together, such that the hedgehog

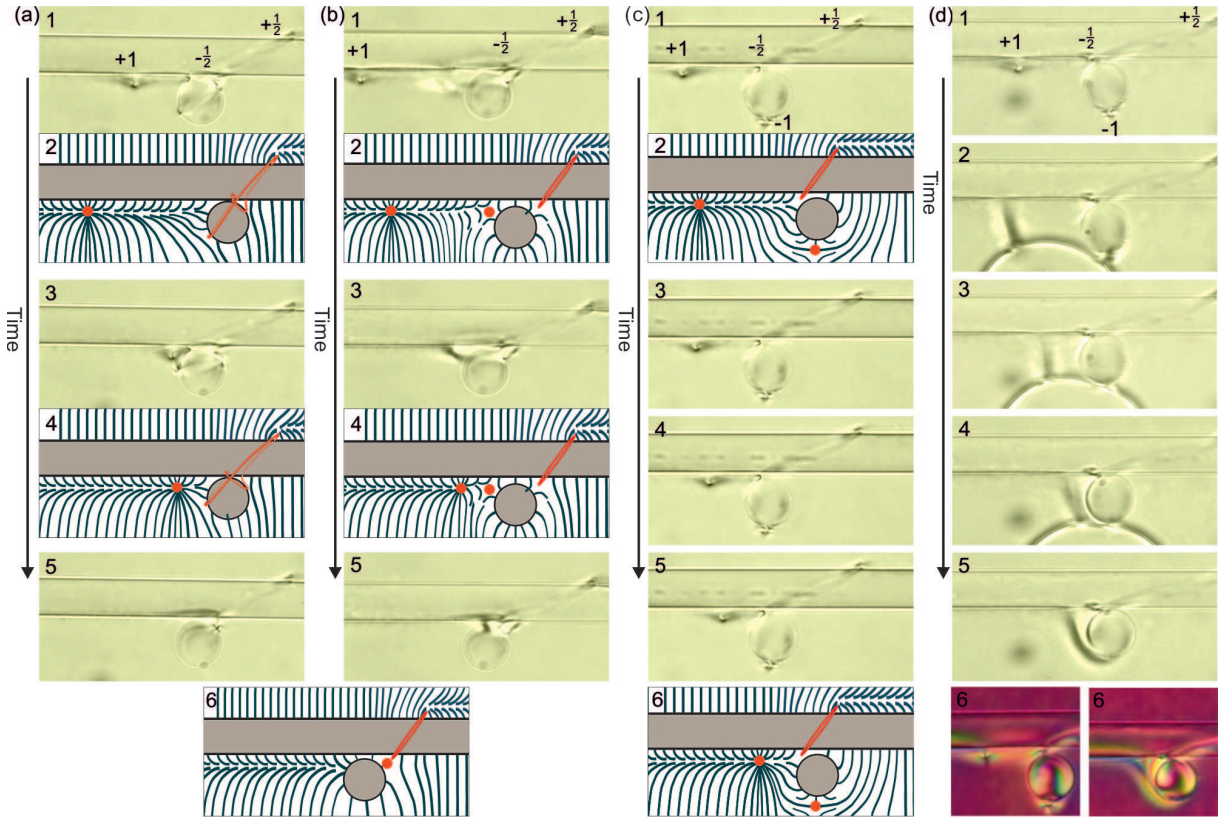

Figure 6. (a) +1 point defect is attracted to the colloidal entanglement know as a figure of omega. Director field around the colloids and point defect is shown schematically in panels 2, 4 and 6. (b) Micro-sphere is bound to the fibre similar to the bubble-gum configuration. The +1 point defect is attracted to the system and changes the entanglement configuration. Panels 2, 4 and 6 show the schematic representation of the director field. (c) In the reversed orientation of the micro-sphere's hedgehog, the + end of the micro-sphere is bound to the - end the loop. The + point defect which is left free in the vicinity of this colloidal binding with the background velocity is far enough from the micro-sphere's hedgehog that it cannot change the system entanglement (see the schematic director field in panels 2 and 6). (d) The fused beam of the laser tweezers is used to push the point defect to sphere, which results in a birefringent vortex-like binding.

point defect on the sphere is sitting in between them. Since the surrounding director field on the right hand side of the microsphere is minimally distorted and continuous, as shown in the second panel of Fig. 5 (a), it dramatically hinders any interaction with other topological defects on that side. This is demonstrated by creating an isolated -1 hedgehog on the left hand side of the colloidal particle. When this -1 point defect is left free, it is repelled from the colloidal particle and the +1/2 segment of the loop. This repulsion between the -1 point defect and the entangled microsphere is further demonstrated by using the laser tweezers to push the -1 point defect towards the entangled structure. To this end, the laser light is focused in the vicinity of the point defect and an isotropic island is created by locally heating the liquid crystal, as shown in the fourth panel of Fig. 5 (a). One can grab and pull the -1 point defect towards the microsphere, as illustrated in the third and fourth panels of Fig. 5 (a). When the tweezers are switched off, there is a clear repulsive elastic force between the microsphere and the -1 point defect and the point defect will start moving away from the colloid, as shown in the fifth and sixth panels of Fig. 5 (a).

Further experiments shown in Fig. 5 (b) reveal that this elastic repulsive barrier between the -1 point and the microsphere can be overcome by using even stronger external force to push the -1 defect towards the joint region between the microsphere and the loop. In this case another energetically favorable configuration can be obtained which is shown in the second and third panel of Fig. 5 (b). Here the laser tweezers is dragging the -1 point defect towards the joint between the -1 hyperbolic hedgehog of the microsphere and the +1/2 segment of the loop on the fibre. At some moment (third panel in Fig. 5 (b)) when the hyperbolic defect reaches the vicinity of the -1 defect of the microsphere, both -1 defects become blurred and actually disappear. It looks like the two hyperbolic -1 point defect have merged into a vortex-like binding, also known as a "bubble-gum" defect [55–57]. This bubble gum defect, also called hyperbolic vortex, is a nonsingular topological structure, which provides extremely strong binding, in this case between the fibre and the microsphere.

Next, we study the interaction of a +1 point defect with the colloidal particle attracted to the -1/2 end of the loop encircling the fibre. It turns out that there are 3 possible types of binding of a dipolar colloidal microsphere to the -1/2 end of the loop: (i) Figure of Omega entanglement [58], (ii) vortex-like binding, and (iii)binding with the + end of the elastic dipole of the microsphere to the -1/2 end of the loop.

Fig. 6(a) shows the first type of binding, which is the entanglement of the -1/2 Saturn ring of the microsphere to the to the negative end of the loop encircling the fibre. One can see that the fibre and the micro-sphere are entangled with a single loop encircling the colloidal particle with a twist segment between them, which is known as a "Figure of Omega". This kind of entanglement can be also observed for two identical microspheres with -1/2 Saturn rings and was first reported in 2007 [58]. The second panel of 6 (a) shows the schematic drawing of the director field around the microsphere-fibre entanglement and the +1 point defect on the left side. We see in the experiment that in this case the +1 point defect is spontaneously attracted to the colloidal entanglement, which is due to the opposite charge between the positive point defect and the negatively charged loop, encircling the colloidal particle. During this attraction the ring around the micro-sphere starts to move toward the +1 point defect, as shown in the third panel of 6 (a). The microsphere loses the figure of Omega entanglement loop and obtains a topological binding structure that resembles the one in the first panel of Fig. 5 (a) (a binding between the +1/2 end of the loop and the micro-sphere).

Fig. 6 (b) shows the interaction between the +1 point defect with the second kind

of colloidal entanglement that is created between -1/2 loop and an elastic dipole. In this case, a dipolar colloidal particle is attracted with its -1 charged hyperbolic defect to the loop with the same -1/2 half charge. The spontaneous attraction between like topological charges creates a vortex-like or bubble-gum binding. A +1 point defects is released close to this colloidal entanglement using the laser tweezers, which is presented in the first panel of Fig. 6 (b). The second panel in 6 (b) shows the corresponding schematics of the director field and defects. The +1 defect is spontaneously attracted to the bubble-gum binding which can be understood by considering the schematic drawing of the director escape around the entangled structure. The second and fourth panels of Fig. 6 (b) clearly show that the escaped region on the right-hand side of +1 defect and the hyperbolic defect of the particle share the same form of distortion, which means they are attracting each other to minimize their elastic energy. When the defect approaches the colloidal binding, the bubble-gum configuration collapses as illustrated in Fig. 6 (b), sixth panel.

Fig. 6 (c,d) show the interaction of the +1 point defect with an elastic dipole, which is attracted to the -1/2 end of the loop with its + end. In addition we have a +1 point defect, which is released in the vicinity of this configuration, as shown in Fig. 6 (c), first panel and schematically in the second panel of this figure. The dipole and the loop will form a strongly bound system, which repels the +1 point defect. However, one can apply an additional force to the +1 point defect by slightly rotating the fibre with respect to the far-field nematic director. Such an offset in the angle gives the topological point defect an additional elastic force, which pushes the defect to achieve a constant velocity v_c, as explained in detail elsewhere [45]. The origin of this additional and constant force can be understood by considering the elastic deformation of the director field around the point defect. The point defect is surrounded by two regions of topological soliton, in which each of these soliton regions represents an elastic string that is pulling the point defect in a direction which minimizes its elastic energy. In this specific case the elastic distortion on the right side of the point defect is more distorted than the left side. Because of the higher elastic distortion, a structural force is created, which tends to minimize this energetically high-cost region, and the point defect starts moving to the right (see Fig. 6 (c), third to fifth panels). On the other hand, there is a very strong repulsive force in the vicinity of the sphere due to the elastic deformation of the director field around the micro-sphere. At a certain point these two forces puling the point defect to the right and left become equal, and the point defect will be stabilized in the vicinity of the micro-sphere, as shown in the Fig. 6 (c), fifth panel and schematically in sixth panel. We can now use the laser tweezers to grab the +1 point defect and move it towards the micro-sphere, as illustrated in Fig. 6 (d). The thermally induced local melting of the liquid crystal (from the nematic to isotropic) changes the elastic deformation of the director field around the sphere and a birefringent, string-like structure is formed, shown in the last colour panel of Fig. 6 (d).

It is difficult to determine from these photos in the last, colour panel of Fig. 6 (d) what kind of defect, if any, is here present. There are two possible scenarios of possible structures, which could be obtained by forcing (and eventually fusing) together the +1 defect coming from the soliton and the -1 hyperbolic belonging to the microsphere. This is analysed in Fig. 7, where the steps of smoothing the director field are performed and presented, which bring together the two point defects. Figs. 7 (a-c) show this process of bringing the +1 and -1 defect close together, which is also shown in the last schematic panel of Fig. 6 (c). Now, there are two options from the situation shown in Fig. 7(c): (i) The two defects could be merged together via an escape mechanism

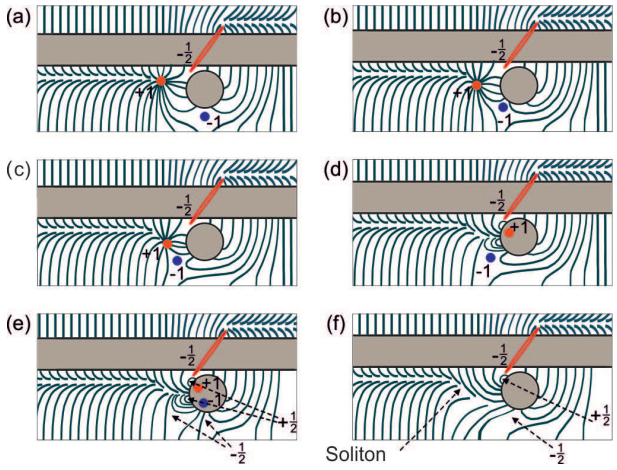

Figure 7. Possible scenarios of the interaction of a +1 point defect with a dipolar microsphere, attached to the -1/2 end of the loop encircling the fibre across the short axis. (a) The initial situation. (b, c) The +1 and -1 points are attracting and approaching each other. (d) The +1 point "sinks" into the microsphere and leaves behind two +1/2 surface defects. (e) The -1 defect also "sinks" into the sphere and leaves behind two -1/2 surface defects. (f) Half-integer defects can pairwise annihilate and leave behind an oppositely charged pair of half-integer defects.

into a bubble gum (or vortex) with charge zero, or (ii) The two point defects could partially annihilate, as shown in panels Fig. 7 (d-f). The first scenario has never been demonstrated before, as the vortex formation has been demonstrated for two equal, -1 charges. In this scenario, a vortex should be created from opposite charges, -1 and +1, which has not been analysed yet theoretically.

As far as the second option is concerned, we see in panels Fig. 7 (d-f) that one can get rid of the two point charges by depressing them into the sphere and preserving the continuity of the director streamlines. One ends in a situation shown in Fig. 7(f), where the two boojums have gone and what is left are small regions close to the colloidal surface of winding +1/2 and -1/2, therefore preserving the total winding of zero. In this case the most pronounced structure is the topological soliton, which comes very close to the colloidal surface. It should be noted that these are only conjectures, which have to be supported by numerical simulations in future.

7. Conclusions

This work demonstrates a surprising variety of topological states of two topologically simple objects, i.e. a microsphere and a microfibre in a planar nematic cell. Contrary to intuition, we observe that the richest topology is obtained in the geometry, where the fibre is set perpendicular to the far field director. In this way, a kind of frustrated situation is realized, where the topological defects are created and partially stabilized in the very vicinity of the fibre. We have shown that defects are easily created in the region of the topological soliton, i.e. the topologically trivial region where no defects are initially present. Most interestingly, we have seen for the first time topological defects that encircle the fibre which is set perpendicular to the far field director of the planar or homeotropic cell. These are either charged or zero topological charge loops encircling the fibre, which are very stable and cannot annihilate to vacuum. We are able to change the topological charge of these loops encircling the fibre simply by

adding extra defects. In all cases we observe conservation of the topological charge, as expected. It should be noted that numerical analysis of the possible topological states is needed to completely clarify the structure of defects or groups of defects, observed in this study. In some cases it is not quite possible to give a definite answer just by optical microscope observations and Landau-de Gennes simulations could resolve this uncertainty as demonstrated in several previous studies.

Acknowledgement(s)

This work was supported by the University of Leeds (M. N.) and the Slovenian Research Agency (ARRS) contract P1-0099 (I. M.).

Disclosure statement

No potential conflict of interest was reported by the authors.

Funding

This work was supported by the University of Leeds (M. N.) and the Slovenian Research Agency (ARRS) contract P1-0099 (I. M.).

8. References

References

[1] Bates AD, Maxwell A, DNA topology. Oxford (UK): Oxford University Press; 2005.
[2] Weiler CN, Neely TW, Scherer DR, et al. Spontaneous vortices in the formation of BoseEinstein condensates. Nature. 2008;455:948-951.
[3] Doostmohammadi A, Thampi SP, Yeomans JM. Defect-Mediated Morphologies in Growing Cell Colonies. Phys. Rev. Lett. 2016;117:048102.
[4] Kibble TWB. Topology of cosmic domains and strings. J. Phys. A: Math. Gen. 1976;9:1387-1398.
[5] Zurek WH. Cosmological experiments in condensed matter systems. Phys. Rep. 1996;276:177-221.
[6] Wachowiak A, Wiebe J, Bode M, et al. Direct observation of internal spin structure of magnetic vortex cores. Science. 2002;298:577-580.
[7] Tchernyshyov O, Chern G-W. Fractional vortices and composite domain walls in flat nanomagnets. Phys. Rev. Lett. 2005;95:197204.
[8] Choe S-B, Acremann Y, Scholl A, et al. Vortex core-driven magnetization dynamics. Science. 2004;304:420-422.
[9] Mermin ND, Ho, T-L. Circulation and angular momentum in the A phase of superfluid helium-3. Phys. Rev. Lett. 1976;36:594-597.
[10] Ruutu VMH, Eltsov VB, Gill AJ, et al. Vortex formation in neutron-irradiated superfluid 3He as an analogue of cosmological defect formation. Nature. 1996;382:334-336.
[11] Bishop DJ, Gammel PL, Huse DA, et al. Magnetic flux line lattices and vortices in the copper oxide superconductors. Science. 1992;255:165-172.
[12] Kurik MV, Lavrentovich OD. Defects in liquid crystals: homotopy theory and experimental studies. Sov. Phys. Usp. 1988;154:381-431.

[13] Alexander GP, Chen BG, Matsumoto EA, et al. Disclination loops, point defects, and all that in nematic liquid crystals. Rev. Mod. Phys. 2012;84:497-514.
[14] Mermin ND. The topological theory of defects in ordered media. Rev. Mod. Phys. 1979;51:591-603.
[15] Chaikin PM, Lubensky TC. Principles of Condensed Matter Physics. Cambridge (UK): Cambridge University Press; 1995.
[16] Muševič I. Liquid Crystal Colloids. Cham: Springer; 2017.
[17] Kleman M, Lavrentovich OD. Topological point defects in nematic liquid crystals. Philos. Mag. 2006;86:4117-4137.
[18] Copar S. Topology and geometry of nematic braids. Phys. Rep. 2014;538:1-37.
[19] Lydon JE, Gleeson H, Jull EIL. The identification of the sign and strength of disclinations in the schlieren (nucleated domain) texture of the nematic phase, by optical microscopy. Liq. Cryst. 2017;44:17751786.
[20] Senyuk B, Liu Q, He S, et al. Topological colloids. Nature. 2013;493:200-205.
[21] Posnjak G, Copar S, Muševič I. Points, skyrmions and torons in chiral nematic droplets. Sci Rep. 2016;6:26361.
[22] Posnjak G, Copar S, Muševič, I. Hidden topological constellations and polyvalent charges in chiral nematic droplets. Nat. Commun. 2017;8:14594.
[23] Škarabot M, Muševič I. Direct observation of interaction of nanoparticles in a nematic liquid crystal. Soft Mat. 2010;6:5476-5481.
[24] Senyuk B, Smalyukh I. Elastic interactions between colloidal microspheres and elongated convex and concave nanoprisms in nematic liquid crystals. Soft Mat. 2012;8:8729-8734.
[25] Dontabhaktuni J, M Ravnik M, Žumer S. Shape-tuning the colloidal assemblies in nematic liquid crystals. Soft Mat. 2012;8:1657-1663.
[26] Nikkhou M, Škarabot M, Čopar S, et al. Light-controlled topological charge in a nematic liquid crystal. Nat. Phys. 2015;11:183-187.
[27] Hashemi SM, Jagodič U, Mozaffari MR, et al Fractal nematic colloids. Nat. Commun. 2017;8:14026.
[28] Gu Y, Abbott NL. Observation of Saturn-Ring Defects around Solid Microspheres in Nematic Liquid Crystals. Phys. Rev. Lett. 2000;85:4719.
[29] Poulin P. Novel phases and colloidal assemblies in liquid crystals. Curr. Opin. Colloids Interface Sci. 1999;4:66-71.
[30] Andrienko D, Allen MP, Skacej G, et al. Defect structures and torque on an elongated colloidal particle immersed in a liquid crystal host. Phys. Rev. E. 2002;65:041702.
[31] Tkalec U, Škarabot M, Muševič I. Interactions of micro-rods in a thin layer of a nematic liquid crystal. Soft Mat. 2008;4:2402-2409.
[32] Muševič I. Optical manipulation and self-assembly of nematic colloids: colloidal crystals and superstructures. Liq. Cryst. Today. 2010;19:2-12.
[33] Muševič I, Škarabot M, Tkalec U, et al. Two-dimensional nematic colloidal crystals self-assembled by topological defects. Science. 2006;313:954-958.
[34] Škarabot M, Ravnik M, Žumer S , et al. Interactions of quadrupolar nematic colloids. Phys. Rev. E. 2008;77:031705.
[35] Serra F. Curvature and defects in nematic liquid crystals. Liq. Cryst. 2016;43(13-15):1920-1936.
[36] Poulin P, Stark H, Lubensky TC, et al. Novel Colloidal Interactions in Anisotropic Fluids. Science. 1997;275:1770-1773.
[37] Loudet JC, Poulin P, Barois P. Edge dislocations of colloidal chains suspended in a nematic liquid crystal. Euro phys. Lett. 2001;54:175.
[38] Loudet JC, Barois P, Poulin P. Colloidal ordering from phase separation in a liquid-crystalline continuous phase. Nature. 2000;407:pages 611613.
[39] Škarabot M, Ravnik M, Žumer S, et al. Entangled Nematic Colloidal Dimers and Wires. Phys. Rev. E. 2007;76:051406.
[40] Nych AB, Ognysta UM, Pergamenshchik VM, et al. Coexistence of Two Colloidal Crystals at the Nematic-Liquid-CrystalAir Interface. Phys. Rev. Lett. 2007;98:057801.

[41] Muševič I, Škarabot M. Self-assembly of nematic colloids. Soft Mat. 2008;4:195-199.
[42] Ognysta U, Nych A, Nazarenko V, et al. 2D Interactions and Binary Crystals of Dipolar and Quadrupolar Nematic Colloids. Phys. Rev. Lett. 2008;100:17803.
[43] Nych A, Ognysta U, Škarabot M, et al. Assembly and control of 3D nematic dipolar colloidal crystals. Nat. Commun. 2013;4:1489.
[44] Nikkhou M, Škarabot M, Čopar S, et al. Dynamics of topological monopoles annihilation on a fibre in a thick and thin nematic layer. Eur. phys. J. E. 2016;39:100.
[45] Nikkhou M, Škarabot M, Muševič I. Annihilation dynamics of topological monopoles on a fiber in nematic liquid crystals. Phys. Rev. E. 2016;93:062703.
[46] Nikkhou M, Škarabot M, Muševič I. Topological binding and elastic interactions of microspheres and fibres in a nematic liquid crystal. Eur. Phys. J. E. 2015;38:23.
[47] Mineyev VP, Volovik GE. Planar and linear solitons in superfluid ^3He. Phys. Rev. B. 1978;7:3197.
[48] Chandrasekhar S, Ranganath GS. The structure and energetics of defects in liquid crystals. Adv. in Phys. 1986;35:507-596.
[49] Kleman M, Laverntovich OD. Soft Matter Physics: An Introduction. New York (NY): Springer; 2006.
[50] Minoura K, Kimura Y, Ito K, et al. Annihilation of a wedge disclination pair in a hybrid aligned nematic cell Phys. Rev. E. 1998;58:643.
[51] Nakata M, Link DR, Araoka F, et al. A racemic layer structure in a chiral bent-core ferroelectric liquid crystal. Liq. Cryst. 2001;28:1301-1308.
[52] Dierking I, Ravnik M, Lark E, et al. Anisotropy in the annihilation dynamics of umbilic defects in nematic liquid crystals Phys. Rev. E. 2012;85:021703.
[53] Heck B van, Burrello M, Yacoby A, et al. Topological Blockade and Measurement of Topological Charge. Phys. Rev. Lett. 2013;110:086803.
[54] Chuang I, Durrer R, Turok N, et al. Cosmology in the Laboratory: Defect Dynamics in Liquid Crystals. Science. 1991;251:1336-1342.
[55] Poulin P, Cabuil V, Weitz DA. Direct Measurement of Colloidal Forces in an Anisotropic Solvent. Phys. Rev. Lett. 1997;79:4862.
[56] Fukuda J-i, Yokoyama H. Separation-Independent Attractive Force between Like Particles Mediated by Nematic-Liquid-Crystal Distortions. Phys. Rev. Lett. 2005;94:148301.
[57] Tkalec U, Ravnik M, Žumer, et al. Vortexlike Topological Defects in Nematic Colloids: Chiral Colloidal Dimers and 2D Crystals. Phys. Rev. Lett. 2009;103:127801.
[58] Ravnik M, Škarabot M, Žumer S, et al. Entangled nematic colloidal dimers and wires. Phys. Rev. Lett. 2007;99:247801.